

A Wideband Line/Cable Model for Real-Time Simulations of Power System Transients

Octavio Ramos-Leaños, José Luis Naredo, *Senior Member, IEEE*, Jean Mahseredjian, *Senior Member, IEEE*, Christian Dufour, *Member, IEEE*, José Alberto Gutiérrez-Robles, and Ilhan Kocar, *Member, IEEE*

Abstract—This paper describes the implementation of a full frequency-dependent model for transmission lines and cables in a state-space-based solver for electromagnetic transients. This implementation is for real-time simulation of power system switching transients. It is based on the wideband universal line model with modifications being incorporated to meet the computational speed requirements of real-time applications. The real-time performance of the implementation is demonstrated through application examples.

Index Terms—Cables, real-time simulation, transients, transmission lines, wideband (WB).

I. INTRODUCTION

AN electromagnetic disturbance occurring at one end of a transmission line reaches the other end after a time delay. This is due to the travel time of electromagnetic waves and the two ends are said to be decoupled in time. This delay effect has been conveniently applied in the partitioning of large power networks for parallel and real-time simulations of electromagnetic transients (EMTs).

Most line models adapted for real-time simulation of EMTs are based on [1] (see [2]–[4]). Frequency-dependent line (FD-Line) models [1] are especially important in real-time simulations due to their good numerical performance and accuracy when dealing with symmetric and nearly symmetric overhead lines [5]. Although these lines are very common, there are many cases involving highly asymmetric overhead lines as well as underground and submarine cables, which cannot be simulated reliably with the FD-Line approach. These cases require that a full-frequency-dependent line model be implemented for real-time simulations.

The main purpose of this paper is to present a full-frequency-dependent model for lines and cables that executes in real time.

Manuscript received January 06, 2012; revised May 06, 2012; accepted June 24, 2012. Date of publication August 08, 2012; date of current version September 19, 2012. This work was supported in part by an NSERC-CRD Grant with Opal-RT and in part by the Mexican Science and Technology Council (CONACYT). Paper no. TPWRD-00017-2012.

O. Ramos-Leaños, J. Mahseredjian and I. Kocar are with the Electrical Engineering Department, École Polytechnique de Montréal, Campus Université de Montréal, Montréal, QC H3T 1J4 Canada (e-mail: jeanm@polymtl.ca).

J. L. Naredo is with the Electrical Engineering Department, Cinvestav, Guadalajara 45015, Mexico (e-mail: jlnaredo@gdl.cinvestav.mx).

C. Dufour is with Opal-RT Technologies Inc., Montreal, QC H3K 1G6 Canada (e-mail: christian.dufour@opal-rt.com).

J. A. Gutiérrez-Robles is with the Department of Mathematics, CUCEI, Universidad de Guadalajara, Guadalajara 45015, Mexico (e-mail: jose.gutierrez@cucei.udg.mx).

Color versions of one or more of the figures in this paper are available online at <http://ieeexplore.ieee.org>.

Digital Object Identifier 10.1109/TPWRD.2012.2206833

The model is targeted for a hardware platform based on clusters of conventional multicore processors. In this paper, the model is implemented into the state-space-based power system simulation environment of Simulink [6] used for real-time computations in [7].

The model reported here is based on the principles of the wideband (WB) or universal line model (ULM) [8]–[11] with various modifications to attain the computational speed required in real-time applications. This model is called real-time wideband (RTWB). It is implemented and tested in the RT-LAB software platform [7].

An important modification introduced in RTWB consists in the handling of all internal state variables of the model by procedures in real arithmetic. In standard WB line/cable model implementations in EMT-type programs, all state variables are treated as complex. It is shown in this paper that through the use of real arithmetic processes, a large number of trivial and redundant computations are eliminated. Additional computational speed improvements for updating internal state variables are also presented.

The computational speed improvements presented in this paper for real-time simulations, can be also reused for offline simulation tools.

This paper also demonstrates that it is possible to include ULM equations into a state-space-based formulation through the usage of the interface proposed in [12].

An additional contribution of this paper is the identification of conditions for instability due to modal grouping normally used for computational efficiency.

A major motivation to pursue real-time simulation of transients is to conduct hardware-in-the loop (HIL) simulations for testing external physical components, such as control systems. This paper focuses on the real-time simulation of switching transients involved in HIL applications.

II. WB MODEL EQUATIONS

A. Main Line/Cable Model Equations

Fig. 1 depicts a power transmission line of length L formed by N parallel conductors. This multiconductor representation can represent an aerial line or an underground or submarine cable.

The steady-state line-end current and voltage phasors are related as follows [8]:

$$\mathbf{I}_0 - \mathbf{Y}_c \mathbf{V}_0 = -\mathbf{H}(\mathbf{I}_L + \mathbf{Y}_c \mathbf{V}_L) \quad (1)$$

$$\mathbf{I}_L - \mathbf{Y}_c \mathbf{V}_L = -\mathbf{H}(\mathbf{I}_0 + \mathbf{Y}_c \mathbf{V}_0) \quad (2)$$

where \mathbf{I}_0 and \mathbf{I}_L are the vectors of injected currents, and \mathbf{V}_0 and \mathbf{V}_L are nodal voltage vectors. The subscript 0 is used for

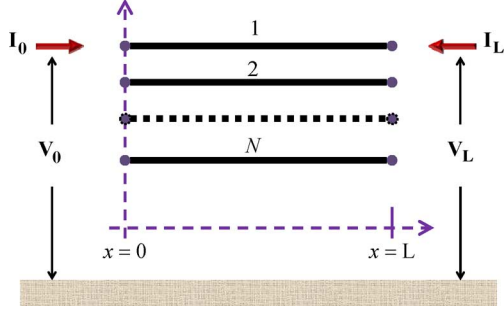


Fig. 1. Multiconductor line segment of length L .

variables at $x = 0$ and the subscripts L stands for variables at $x = L$. The characteristic admittance matrix \mathbf{Y}_c is given by

$$\mathbf{Y}_c = \mathbf{\Gamma} \mathbf{Z}^{-1} \quad (3)$$

with $\mathbf{\Gamma} = \sqrt{\mathbf{Y}\mathbf{Z}}$, \mathbf{Y} , and \mathbf{Z} are $N \times N$ -coupled matrices per unit length representing shunt admittances and series impedances, respectively. These two matrices can be obtained with the line and cable constants utilities available in electromagnetic-transient (EMT)-type programs. \mathbf{H} is the propagation matrix given by

$$\mathbf{H} = e^{-\mathbf{\Gamma}L}. \quad (4)$$

In (1), the term $\mathbf{Y}_c \mathbf{V}_0$ is considered as a shunt current

$$\mathbf{I}_{sh0} = \mathbf{Y}_c \mathbf{V}_0 \quad (5)$$

whereas the right-hand side is denoted by

$$\mathbf{I}_{H0} = \mathbf{H}(\mathbf{I}_L + \mathbf{Y}_c \mathbf{V}_L) = \mathbf{H} \mathbf{I}_{fwL} \quad (6)$$

where \mathbf{I}_{fwL} is the forward traveling current-wave vector from the L side. The time-domain versions of (1), (5), and (6) result in

$$\mathbf{i}_0 = \mathbf{i}_{sh0} - \mathbf{i}_{H0} \quad (7)$$

$$\mathbf{i}_{sh0} = \mathbf{y}_c \otimes \mathbf{v}_0 \quad (8)$$

$$\mathbf{i}_{H0} = \mathbf{h} \otimes \mathbf{i}_{fwL} = \mathbf{h} \otimes (\mathbf{i}_L + \mathbf{y}_c \otimes \mathbf{v}_L) \quad (9)$$

where the lowercase variables represent the time-domain versions of their uppercase counterparts and the symbol \otimes indicates convolution. Equations (7)–(9) provide the time-domain model of the line at $x = 0$. They can be directly inserted into a nodal analysis formulation of the main network equations.

Expressions similar to (5)–(9) can be written for the right-hand side ($x = L$) by interchanging subscripts 0 and L .

B. State-Space Form for Characteristic Admittance Matrix

The convolutions in (8) and (9) are carried out conveniently through the state-space relations that arise when matrices \mathbf{Y}_c and \mathbf{H} are represented by rational functions [13]. A state-space form for (8) is derived next by means of the following rational representation [8]:

$$\mathbf{Y}_c = \mathbf{G}_0 + \sum_{i=1}^{N_y} \frac{1}{s - q_i} \mathbf{G}_i \quad (10)$$

where N_y is the order of the fit, q_i represents the i th fitting pole, \mathbf{G}_i is the corresponding matrix of residues, and \mathbf{G}_0 is a constant matrix obtained at the limit of \mathbf{Y}_c when $s = j\omega \rightarrow \infty$. The poles of \mathbf{Y}_c are obtained by applying the (vector fitting) VF technique [14] to the trace of \mathbf{Y}_c [10]. The VF variant developed in [15] and [16] is used in this paper.

When (10) is introduced into (5), then (11) is obtained

$$\mathbf{I}_{sh0} = \mathbf{G}_0 \mathbf{V}_0 + \sum_{i=1}^{N_y} \mathbf{W}_i, \quad \mathbf{W}_i = \frac{1}{s - q_i} \mathbf{G}_i \mathbf{V}_0. \quad (11)$$

This equation can be now written in time domain using the inverse Laplace transform

$$\mathbf{i}_{sh0} = \mathbf{G}_0 \mathbf{v}_0 + \sum_{i=1}^{N_y} \mathbf{w}_i \quad (12)$$

$$\frac{d\mathbf{w}_i}{dt} = q_i \mathbf{w}_i + \mathbf{G}_i \mathbf{v}_0. \quad (13)$$

The trapezoidal integration method is applied to (13) to obtain

$$\mathbf{w}_i = \hat{\mathbf{G}}_i \mathbf{v}_0 + \hat{q}_i \mathbf{w}'_i + \hat{\mathbf{G}}_i \mathbf{v}'_0 \quad (14)$$

where hatted variables result from the discretization process and primed variables denote their past values found at the previous timepoint $t - \Delta t$. It is possible to introduce (14) into (12) directly, but since saving computing time is a key factor in real-time programming, a more efficient approach is based on a change of variable. By realizing that, the history part in (14) is given by

$$\mathbf{w}_{i_{hist}} = \mathbf{w}_i - \hat{\mathbf{G}}_i \mathbf{v}_0 \quad (15)$$

it is possible to introduce a new variable

$$\boldsymbol{\psi}_i = \frac{1}{\hat{q}_i + 1} (\hat{\mathbf{G}}_i^{-1} \mathbf{w}_i - \mathbf{v}_0) \quad (16)$$

$$\boldsymbol{\psi}_i = \hat{q}_i \boldsymbol{\psi}'_i + \mathbf{v}'_0. \quad (17)$$

Finally (12) is rewritten as

$$\mathbf{i}_{sh0} = \mathbf{G} \mathbf{v}_0 + \sum_{i=1}^{N_y} (\hat{q}_i + 1) \hat{\mathbf{G}}_i \boldsymbol{\psi}_i \quad (18)$$

where the constant matrix \mathbf{G} is given by

$$\mathbf{G} = \mathbf{G}_0 + \sum_{i=1}^{N_y} \hat{\mathbf{G}}_i. \quad (19)$$

It is shown in Appendix A that the aforementioned approach reduces the number of floating-point multiplications and additions by nearly half in the time-domain solution loop of the model.

C. State-Space Form for Propagation Matrix

To attain an accurate and compact (low order) rational representation for a matrix function of s , it is essential to factor out all terms involving time delays [1]. The major difficulty with \mathbf{H} is that its elements usually involve a mix of N different delay terms due to multimode propagation on an N -conductor

line [17]. The separation of \mathbf{H} in single-delay terms is obtained through modal factorization [17]

$$\mathbf{H} = \mathbf{T}\mathbf{H}_m\mathbf{T}^{-1} \quad (20)$$

where \mathbf{T} is the matrix of eigenvectors of the $\mathbf{Y}\mathbf{Z}$ product in (4) and \mathbf{H}_m is a diagonal matrix of the form

$$\mathbf{H}_m = \text{diag} \left[e^{(-\gamma_1 L)}, e^{(-\gamma_2 L)}, \dots, e^{(-\gamma_N L)} \right] \quad (21)$$

with γ being the modal propagation constant [17].

It can be shown that (20) can be written as

$$\mathbf{H} = \sum_{i=1}^N \mathbf{D}_i e^{(-\gamma_i L)} \quad (22)$$

where \mathbf{D}_i is the rank-1 matrix obtained by premultiplying the i th column of \mathbf{T} by the i th row of \mathbf{T}^{-1} . \mathbf{D}_i is, in fact, idempotent [18]. Equation (22) can be further decomposed to give

$$\mathbf{H} = \sum_{i=1}^N \mathbf{D}_i e^{(-\tilde{\gamma}_i L)} e^{(-s\tau_i)} = \sum_{i=1}^N \tilde{\mathbf{H}}_i e^{(-s\tau_i)} \quad (23)$$

where τ_i is the time delay associated with the velocity of the i th mode and $\tilde{\gamma}_i$ is the i th modal propagation constant being modified by the delay subtraction. The time delays in (23) can be initially estimated by applying Bode's relation for minimum phase complex functions [19] to the modal exponential factors in (21). Although (23) provides the desired separation of \mathbf{H} as a sum of terms, each one involving a single delay factor, the following consideration is brought in for computational efficiency [8]. Modal delays often occur in groups with almost identical values and whether a set of exponential factors can be grouped or not is determined by comparing the phase shifts associated with their time delays. The set is a delay group if the phase-shift differences are below a pre-established value, typically chosen at 10° at high frequencies [8]. This is the delay grouping method used in standard WB model implementations in EMT-type programs. Nevertheless, an example in Section V-B shows that despite the associated phases of two modal propagation constants being almost identical, their magnitudes can be quite apart, and grouping these constants stiffens the fitting process. This results in poor fitting and, consequently, causes numerical instability problems in the time domain. The number of total poles is not necessarily reduced either with the standard grouping method. The notation that will be used is simplified by not showing delay grouping.

Each term $\tilde{\mathbf{H}}_i$ in (23) can now be fitted as follows:

$$\tilde{\mathbf{H}}_i = \sum_{k=1}^{M_i} \frac{1}{s - p_{i,k}} \mathbf{R}_{i,k} \quad (24)$$

where M_i is the order of the fit for the i th term $\tilde{\mathbf{H}}_i$; $p_{i,k}$ represents its k th fitting pole and $\mathbf{R}_{i,k}$ is a matrix of residues determined by a fitting process (see [10] and [13]–[16]). The matrices $\tilde{\mathbf{H}}_i$ are obtained from \mathbf{H} by a modal decomposition as in (20). It is required that through all of the frequencies being considered in the fitting process, the transformation matrix \mathbf{T} preserves the same eigenvector (column) order. Since the diagonalizing procedures used to obtain the \mathbf{T} matrices cannot guarantee this,

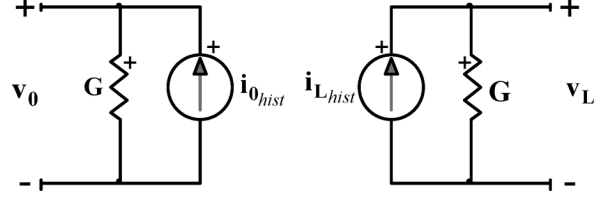


Fig. 2. Discrete time-domain circuit representation of a multiconductor line.

a subsequent reordering process must be employed. The latter process is usually based on the mode tracking by the correlation method described in [22].

Equation (24) is combined with (23) and inserted into (6) to give

$$\mathbf{I}_{\mathbf{H}_0} = \sum_{i=1}^N \left(\sum_{k=1}^{M_i} \frac{1}{s - p_{i,k}} \mathbf{R}_{i,k} \right) e^{(-s\tau_i)} \mathbf{I}_{\mathbf{f}_{\mathbf{W}L}} = \sum_{i=1}^N \sum_{k=1}^{M_i} \mathbf{X}_{i,k} \quad (25)$$

where

$$\mathbf{X}_{i,k} = \frac{1}{s - p_{i,k}} \mathbf{R}_{i,k} \mathbf{I}_{\mathbf{f}_{\mathbf{W}L}} e^{(-s\tau_i)}. \quad (26)$$

The inverse Laplace transform is applied to (25) and (26) to give

$$\mathbf{i}_{\mathbf{H}_0} = \sum_{i=1}^N \sum_{k=1}^{M_i} \mathbf{x}_{i,k} \quad (27)$$

$$\frac{d\mathbf{x}_{i,k}}{dt} = p_{i,k} \mathbf{x}_{i,k} + \mathbf{R}_{i,k} \mathbf{i}_{\mathbf{f}_{\mathbf{W}L}}(t - \tau_i). \quad (28)$$

At this stage, the above equation is discretized directly using the trapezoidal integration rule

$$\mathbf{x}_{i,k} = \hat{p}_{i,k} \mathbf{x}'_{i,k} + \hat{\mathbf{R}}_{i,k} [\mathbf{i}_{\mathbf{f}_{\mathbf{W}L}}(t - \tau_i) + \mathbf{i}'_{\mathbf{f}_{\mathbf{W}L}}(t - \tau_i)] \quad (29)$$

where the primed and hatted notations are similar to (14). Hence, (29) provides the update of state vectors $\mathbf{x}_{i,k}$ using only past values of variables already available, either from initial conditions or from previous simulation timepoints.

D. Complete Model

The equivalent circuit model shown in Fig. 2 results from the introduction of (18) and (27) into (7). The \mathbf{G} matrix is given by (19) and the history current is the combined equation

$$\mathbf{i}_{0_{hist}} = \sum_{i=1}^{N_y} (\hat{q}_i + 1) \hat{\mathbf{G}}_i \boldsymbol{\psi}_i - \sum_{i=1}^N \sum_{k=1}^{M_i} \mathbf{x}_{i,k}. \quad (30)$$

A similar equation can be written for $x = L$.

III. STATE-SPACE ANALYSIS WITH REAL ARITHMETIC

Since VF is applied to obtain rational approximations of \mathbf{Y}_c and \mathbf{H} , some of the fitting poles can be complex. These poles and their associated state variables come in conjugate pairs. The imaginary parts of the state variables must cancel (each other) at the sums in (30). In a direct implementation of the WB model, as described in the previous section, all internal state variables are treated as complex including those that are real. This approach is, in fact, the one adopted in standard implementations of the WB model in EMT-type programs. From the standpoint of

computational efficiency for a real-time code, however, this direct approach introduces a large number of trivial and redundant computations [20], even if a given fitting is achieved without complex poles.

In these authors' experience, complex poles arise less frequently in the fitting of \mathbf{Y}_c than in the one of \mathbf{H} . For the two test cases shown in Section V, one for an underground cable and the other for an aerial line, the two admittance matrices were fitted with real poles only. As for the propagation matrices, 20% of the poles were complex for the underground cable, while for the aerial line, only two out of 30 poles (7%) were complex.

Thus, the handling of the real variables as complex variables will increase the number of sums at least by a factor of two and the number of real multiplications by a factor of four. In addition, all of the added sums and multiplications are trivial; that is, sums of zeros and multiplications by zeros. For the case of complex state variables, the two states from a conjugate pair convey the same information and the computation of these two is redundant. In the WB model implementation reported here, redundant states are eliminated and each remaining complex state is handled as a pair of coupled real states. The proposed modification enables achieving a typical gain of at least two in computational speed. It can equally impact real-time and offline implementations.

Assume that two fitting poles in (11) or in (25) are complex conjugates. This means that $\rho = \rho_R + j\rho_I$ and $\rho^* = \rho_R - j\rho_I$, using subscripts R for real and I for imaginary parts. The generic letter ρ is used here to designate an arbitrary pole. The contribution of those complex poles to the output equation, either (11) or (25), is given in generic terms as

$$\mathbf{I}_D = \mathbf{D}_1 + \mathbf{D}_2 \quad (31)$$

where

$$\mathbf{D}_1 = (s - \rho)^{-1} \mathbf{B} \mathbf{U}, \quad \mathbf{D}_2 = (s - \rho^*)^{-1} \mathbf{B}^* \mathbf{U} \quad (32)$$

where \mathbf{B} is a member of \mathbf{G} in (11) or a member of \mathbf{R} in (25), and $\mathbf{U} = \mathbf{V}_0$ in (11) or $\mathbf{U} = e^{(-s\tau_i)} \mathbf{I}_{fwL}$ in (25). The application of the inverse Laplace transform to (31) and (32) yields

$$\mathbf{i}_D = \mathbf{d}_1 + \mathbf{d}_2 \quad (33)$$

$$\dot{\mathbf{d}}_1 = \rho \mathbf{d}_1 + \mathbf{B} \mathbf{u} \quad (34)$$

$$\dot{\mathbf{d}}_2 = \rho^* \mathbf{d}_2 + \mathbf{B}^* \mathbf{u}. \quad (35)$$

Consideration is made now as to the fact that

$$\mathbf{d}_1 = \mathbf{d}_R + j\mathbf{d}_I, \quad \mathbf{d}_2 = \mathbf{d}_R - j\mathbf{d}_I. \quad (36)$$

On introducing (36) into (33)

$$\mathbf{i}_D = 2\mathbf{d}_R. \quad (37)$$

The replacement of (36) into (34) results into the following pair of coupled differential equations:

$$\begin{bmatrix} \dot{\mathbf{d}}_R \\ \dot{\mathbf{d}}_I \end{bmatrix} = \begin{bmatrix} \rho_R & -\rho_I \\ \rho_I & \rho_R \end{bmatrix} \begin{bmatrix} \mathbf{d}_R \\ \mathbf{d}_I \end{bmatrix} + \begin{bmatrix} \mathbf{B}_R \\ \mathbf{B}_I \end{bmatrix} \mathbf{u}. \quad (38)$$

The same equation is obtained when replacing (36) into (35). It is thus clear that (35) is redundant, and (37) and (38) are suffi-

cient to determine the output \mathbf{i}_D . In addition, the state vectors \mathbf{d}_R and \mathbf{d}_I are real.

At this stage, trapezoidal integration is used again to discretize (38)

$$\mathbf{d}_R = \mathbf{C} \mathbf{u} + \alpha \mathbf{d}'_R - \beta \mathbf{d}'_I + \mathbf{C} \mathbf{u}' \quad (39)$$

$$\mathbf{d}_I = \mathbf{E} \mathbf{u} + \alpha \mathbf{d}'_I + \beta \mathbf{d}'_R + \mathbf{E} \mathbf{u}'. \quad (40)$$

The coefficients \mathbf{C} , \mathbf{E} , α , and β are given by

$$\mathbf{C} = \frac{[(2\Delta t - \Delta t^2 \rho_R) \mathbf{B}_R - \Delta t^2 \rho_I \mathbf{B}_I]}{k} \quad (41)$$

$$\mathbf{E} = \Delta t^2 \rho_I \mathbf{B}_R + (2\Delta t - \Delta t^2 \rho_R) \mathbf{B}_I / k \quad (42)$$

$$\alpha = 1 + [4\Delta t \rho_R - 2\Delta t^2 (\rho_R^2 + \rho_I^2)] / k \quad (43)$$

$$\beta = \frac{4\Delta t \rho_I}{k} \quad (44)$$

with $k = 4 - 4\Delta t \rho_R + \Delta t^2 (\rho_R^2 + \rho_I^2)$.

Due to computational speed issues explained before for the programming of (13), a change of variable is also introduced in (39) and (40). The state variables are redefined as follows:

$$\mathbf{y}_R = \mathbf{d}_R - \mathbf{C} \mathbf{v}_0 \quad (45)$$

$$\mathbf{y}_I = \mathbf{d}_I - \mathbf{E} \mathbf{v}_0. \quad (46)$$

The introduction of (45) and (46) into (37), (39), and (40) gives

$$\mathbf{i}_D = 2\mathbf{y}_R + 2\mathbf{C} \mathbf{v}_0 \quad (47)$$

$$\mathbf{y}_R = \alpha \mathbf{y}'_R - \beta \mathbf{y}'_I + \tilde{\mathbf{C}} \mathbf{v}'_0 \quad (48)$$

$$\mathbf{y}_I = \alpha \mathbf{y}'_I - \beta \mathbf{y}'_R + \tilde{\mathbf{E}} \mathbf{v}'_0 \quad (49)$$

where $\tilde{\mathbf{C}} = (\alpha + 1)\mathbf{C} - \beta\mathbf{E}$ and $\tilde{\mathbf{E}} = (\alpha + 1)\mathbf{E} + \beta\mathbf{C}$.

On the basis of (47)–(49), (18) and (19) are modified as follows:

$$\mathbf{i}_{sh0} = \mathbf{G} \mathbf{v}_0 + \sum_{i=1}^{N_{yR}} (\hat{q}_i + 1) \hat{\mathbf{G}}_i \boldsymbol{\psi}_i + 2 \sum_{i=1}^{N_{yC}/2} \mathbf{y}_{Ri} \quad (50)$$

$$\mathbf{G} = \mathbf{G}_0 + \sum_{i=1}^{N_{yR}} \hat{\mathbf{G}}_i + 2 \sum_{i=1}^{N_{yC}/2} \mathbf{C}_i. \quad (51)$$

For the case of complex poles in (27), the input \mathbf{u} is an already determined historic value; thus, (27) can be directly modified as follows:

$$\mathbf{i}_{H0} = \sum_{i=1}^N \left(\sum_{k=1}^{M_{iR}} \mathbf{x}_{i,k} + 2 \sum_{k=1}^{\frac{M_{iC}}{2}} \mathbf{x}_{Ri,k} \right) \quad (52)$$

where M_{iR} and M_{iC} are the number of real and complex poles, respectively.

As a final step, the history parts of (50) and (52) are combined to create an improved version for the history current of (30)

$$\mathbf{i}_{ohist} = \sum_{i=1}^{N_{yR}} (\hat{q}_i + 1) \hat{\mathbf{G}}_i \boldsymbol{\psi}_i + 2 \sum_{i=1}^{\frac{N_{yC}}{2}} \mathbf{y}_{Ri} - \sum_{i=1}^N \left(\sum_{k=1}^{M_{iR}} \mathbf{x}_{i,k} + 2 \sum_{k=1}^{\frac{M_{iC}}{2}} \mathbf{x}_{Ri,k} \right). \quad (53)$$

IV. MODEL IMPLEMENTATION IN A REAL-TIME PLATFORM

The WB cable/line model described in Section II with the modifications described in Section III is coded in C language and implemented as an object in the RT-LAB platform [7] (eMEGAsim simulator) for its execution in real time. This constitutes the RTWB line and cable model. Two sub-blocks are used: one for each line/cable end. Each sub-block can be executed in parallel on a different processor of PC-cluster-based hardware. The sub-blocks create natural-network decoupling due to propagation delay between both ends.

The RT-LAB platform is based on the SimPowerSystems toolbox of Simulink [6] and employs a state-space formulation for network equations. The RTWB model, on the other hand, has a nodal formulation. The interfacing of RTWB with RT-LAB is through the state-space nodal (SSN) solver described in [12]. With this approach, the nodal model presented in Fig. 2 can be directly and simultaneously interfaced with the network-state equations using an SSN V-type group [12]. It means that the Norton model of Fig. 2 is directly mapped into the nodal equations of the corresponding nodal group.

The trapezoidal numerical integration method is used in the RTWB model. Network-state-space equations have been also discretized using trapezoidal integration for the presented tests, but other available solution methods can be used since there are no imposed limitations from the RTWB model side.

It is emphasized that inserting the WB model-state equations directly into the network-state equations was not realizable without the SSN method due to the resulting large number of states.

The time-domain solution steps are identical for both sub-blocks, and only the code steps for the $x = 0$ side are given below as follows.

- Step 1) SSN uses history currents (see Fig. 2) known either from initial conditions or from previous simulation steps to determine network voltages \mathbf{v}_0 .
- Step 2) Calculate \mathbf{i}_{sh0} with (50) and save the history part separately.
- Step 3) Calculate \mathbf{i}_{H0} with (52).
- Step 4) Calculate $\mathbf{i}_{fw0} = 2\mathbf{i}_{sh0} - \mathbf{i}_{H0}$ from the combination of (7) and (8), deliver to the $x = L$ side.
- Step 5) Update internal model states.
- Step 6) Calculate $\mathbf{i}_{0,hist}$ using (53).
- Step 7) Go back to Step 1) until the end of the simulation time.

In the update Step 5), (17) and (29) are used for real states. For a given complex state, it is necessary to use (48) and (49) for \mathbf{Y}_c and (39) and (40) for \mathbf{H} .

A key aspect in the development of the RTWB model is the improvement of numerical performance with respect to the original ULM. The model execution time is a critical aspect of real-time simulations for the reason that the simulation process is interfaced with real-world devices through analog and digital converters. These converters and the simulation process driving them are controlled by a real-time clock inside the simulator, it is therefore very important that the calculations of the network solver and in the models be completed at every time step of the simulator. For this reason, in real-time simulation, the

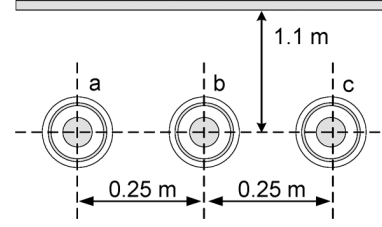


Fig. 3. Underground cable layout for Case 1.

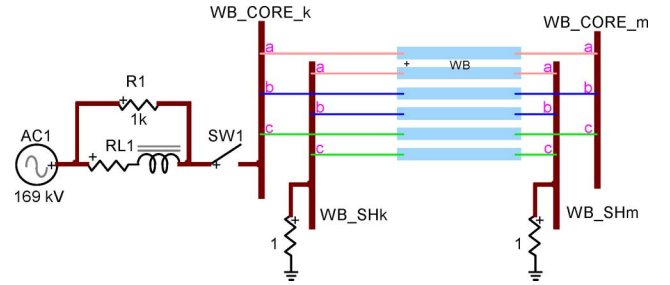


Fig. 4. Case 1 test circuit.

time step is measured as the worst case calculation time for all time steps. Once this worst case time step is known, it is possible to complete all computations in real time and the interface with real-world devices is not disrupted. The RTWB cases presented in the following section were simulated with the real-time clock.

As a byproduct of the aforementioned programming, it was also possible to implement the offline version of the RTWB model into the SimPowerSystems toolbox of Simulink [6] using again the SSN interfacing approach. The code behind each sub-block is an s -function [6] coded in C language.

V. NUMERICAL PERFORMANCE OF RTWB IMPLEMENTATION

The RTWB model has been tested extensively against the offline WB model version available in EMTP-RV [21]. The comparisons included long-term numerical stability and low-frequency performance. The model showed no sign of instability for up to 600 s of simulation time and being excited with steps and sinusoidal functions. In all of these tests, the RTWB model has given accurate results. Real time was achieved using eMEGAsim [7] with two six-core processors (3.33 GHz, Xeon X5680) with a 12-MB L3 cache on each processor.

Two test cases are presented below.

A. Underground Cable, Case 1

The underground cable system used in this test is taken from [15] (see the case shown in Fig. 1, only the left-hand side, with an earth resistivity of 100 Ωm). The cable system layout is shown in Fig. 3. The corresponding electrical circuit diagram is shown in Fig. 4. The circuit parameters are:

- cable length: 15 km;
- cable sheaths are grounded by 1- Ω resistance at both ends;
- ac source AC1: Y-grounded, 169 kV;
- R1 is 1 k Ω ;
- RL1 is determined by its zero-sequence (0) and positive-sequence (1) data in ohms: $R_0 = 2$, $R_1 = 1$, $X_0 = 22$, and $X_1 = 15$;

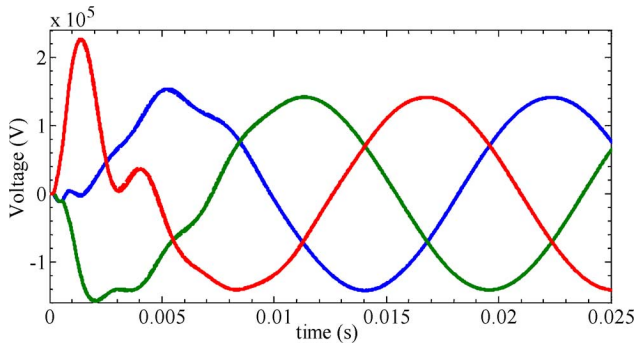


Fig. 5. Core voltages (bus WB_CORE_m in Fig. 4), Case 1, phase-a is red, phase-b is blue, phase-c is green, dashed line is EMTP-RV, solid is eMEGAsim.

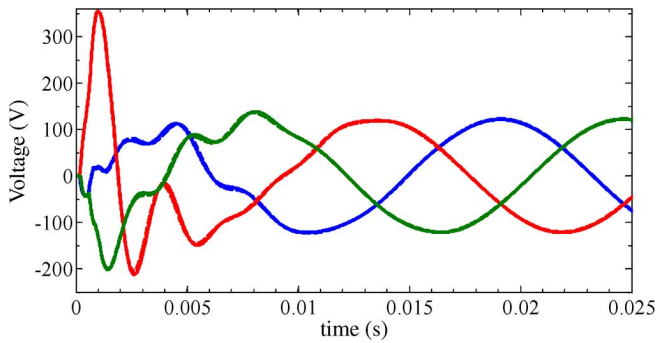


Fig. 6. Sheath voltages (bus WB.SHm in Fig. 4), Case 1, phase-a is red, phase-b is blue, phase-c is green, dashed line is EMTP-RV, solid is eMEGAsim.

- switch SW1 closing times are: 0 s on phase-a, 0.63 ms on phase-b, and 0.4 ms on phase-c.

In this case, the fitting of \mathbf{Y}_c requires 14 real poles and no complex poles, while the fitting of \mathbf{H} requires 30 real poles and 6 complex poles. No delay grouping is needed for \mathbf{H} .

Simulation results are presented in Fig. 5. A dashed line is used for EMTP-RV waveforms and a solid line is for eMEGAsim results. The observed minor differences are related to the different numerical integration techniques used in EMTP-RV and eMEGAsim. The achieved smallest real-time integration timestep is 12 μ s.

This test case is presented without cross-bonding. The reason is that the non-cross-bonded cable poses a more stringent test on the stability of the RTWB model. Nevertheless, the tests were repeated with cross-bonding and the real-time performance of the model has remained equal.

B. Transmission Line, Case 2

The geometry of this test case is shown in Fig. 7. Conductor data can be found in [18] (see Fig. 6). There are three coupled transmission lines. Circuit 1 is composed of conductors 1 to 3, Circuit 2 is for conductors 4 to 6, and Circuit 3 uses conductors 7 to 9. The line length is 150 km.

In Case 2, the fitting of \mathbf{Y}_c requires 9 real poles and no complex poles, while the fitting of \mathbf{H} requires 28 real poles and 2 complex poles without delay grouping.

The magnitudes of \mathbf{H}_m and related phase angles are shown in Figs. 8 and 9. These results are internal to the vector fitting

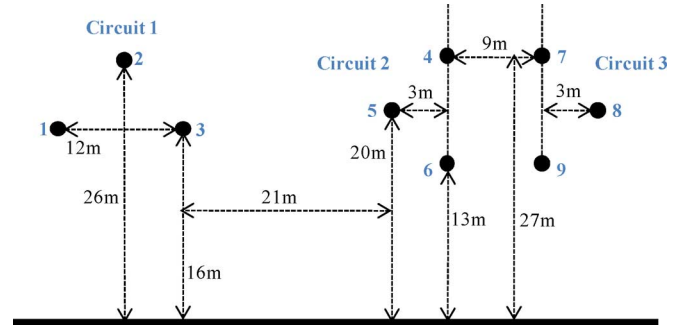


Fig. 7. Transmission-line configuration, Case 2.

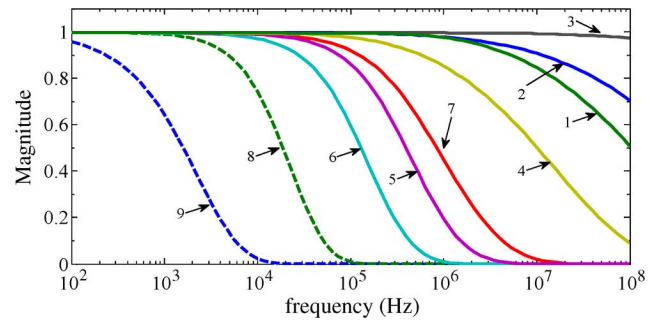


Fig. 8. Magnitudes of \mathbf{H}_m , 9 modes, test Case 2.

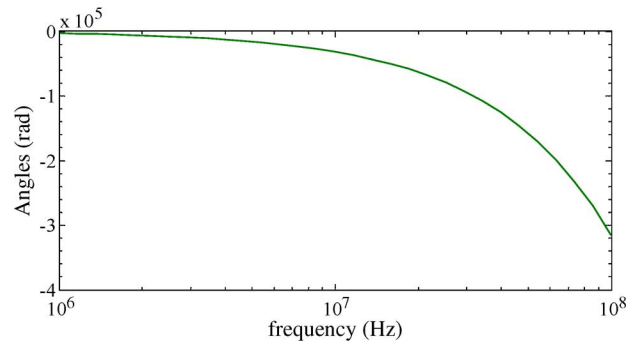


Fig. 9. Phase angles of \mathbf{H}_m , 9 modes, test Case 2.

process. The time delay printouts are listed in Table I. It is apparent that although the phase angles are overlapping, the magnitudes are evidently apart. If modes 1–3 are grouped according to the standard procedure explained in Section II-C, then the solution in time domain becomes numerically unstable. Thus, delay grouping must be turned off in this case.

Since delay grouping was essentially used for computational speed purposes, a more systematic approach must be developed with automatic validation for the grouping criterion. This is to avoid potential numerical stability problems.

The transmission line is energized on Circuit 1 (see Fig. 7) using the same network-side equivalent as in Fig. 4 and the same switch closing timings, except now the system voltage is 230 kV. Simulation results for the receiving end voltages of Circuit 1 are presented in Fig. 10. The simulation waveforms are undistinguishable when comparing EMTP-RV (dashed line) and eMEGAsim (solid line). The lowest achievable real-time timestep in eMEGAsim was 20 μ s.

TABLE I
MODAL TIME DELAYS

Mode	time delays (ms)
1	0.5003398885760
2	0.5003399493433
3	0.5003401639746
4	0.5003418352395
5	0.5003934923478
6	0.5004716033910
7	0.5010042164626
8	0.5070410784460
9	0.5760092190364

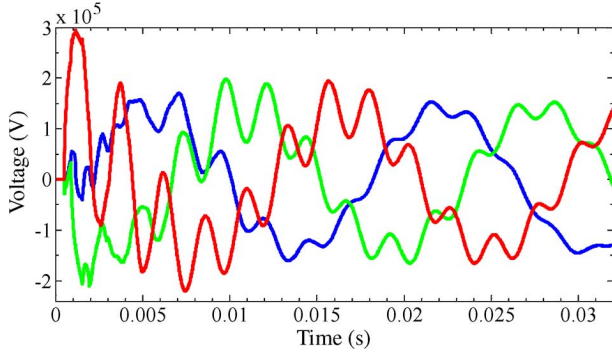


Fig. 10. Circuit 1 receiving end voltages, Case 2 (Fig. 7), phase-a is red, phase-b is blue, phase-c is green, dashed line is EMTP-RV, solid is eMEGAsim.

C. Offline Performance

The standard ULM of EMTP-RV has been used in the previous test cases to validate the results from the RTWB model. Then, the ULM model code of EMTP-RV was upgraded (ULM-new) to include the numerical performance improvements found in this paper for the RTWB model.

For the simulation of Case 1, the standard ULM was executed in 2263 ms, while ULM-new used only 410 ms. For Case 2, the execution time with the standard ULM code was 781 ms and down to 110 ms with the ULM-new version. These offline results imply an increase in numerical performance between 5 to 7 times.

VI. CONCLUSION

An implementation of a model for real-time simulation of electromagnetic transients in power system lines and cables has been presented in this paper. The implementation has been based on the ULM WB model as originally described in [8] and with improvements presented in [15] and [16]. Modifications have been incorporated to attain and optimize real-time performance. One of these modifications has been the handling of complex poles and complex state variable equations by procedures in real arithmetic. The proposed modifications also enable increasing the computational speed in offline simulation methods.

The new real-time wideband (RTWB) model has been implemented in a state-space solver using the SSN interfacing method proposed in [12]. The state-space solver can be used in the offline mode directly within Simulink (SimPowerSystems) and in the real-time mode version in eMEGAsim.

One more contribution is the elimination of numerical stability problems for a practical line energization case. The instability resulted from the propagation matrix modal delay grouping used in the standard vector fitting approach. It should be pointed out here that further research on this topic is being conducted by the authors.

The presented new RTWB model extends the application range of real-time simulation tools for simulation cases requiring wideband line and/or cable models. This is the case, for example, in offshore grid simulation and analysis of EMTs.

APPENDIX A

NUMERICAL PERFORMANCE, STATE SPACE METHODS

Equation (12) has a dimension of $N \times 1$ and can be evaluated using two different methods.

In Method 1, (14) is directly replaced into (12) to give

$$\mathbf{i}_{sh0} = \mathbf{G}\mathbf{v}_0 + \sum_{i=1}^{N_y} \boldsymbol{\eta}_i \quad (54)$$

with the \mathbf{G} matrix given by (19) and $\boldsymbol{\eta}_i = \hat{q}_i \mathbf{w}'_i + \hat{\mathbf{G}}_i \mathbf{v}'_0$. Equation (14) is now written as $\mathbf{w}_i = \hat{\mathbf{G}}_i \mathbf{v}_0 + \boldsymbol{\eta}_i$. The following solution steps are applied at each simulation timepoint and for both sides of the line. Only the left-hand side ($x = 0$) is shown here

- 1) evaluate $\boldsymbol{\eta}_i = \hat{q}_i \mathbf{w}'_i + \hat{\mathbf{G}}_i \mathbf{v}'_0$ for all N_y ;
- 2) evaluate $\sum_{i=1}^{N_y} \boldsymbol{\eta}_i$ in (54);
- 3) provide the history currents of (30) to the network solution to find \mathbf{v}_0 ;
- 4) update $\mathbf{w}_i = \hat{\mathbf{G}}_i \mathbf{v}_0 + \boldsymbol{\eta}_i$ for all N_y ;
- 5) prepare for the next timepoint $\mathbf{w}'_i = \mathbf{w}_i$ and $\mathbf{v}'_0 = \mathbf{v}_0$.

The number of multiplications and additions per timepoint are given by the same count $N_y * N * (2N + 1)$.

In Method 2, (18) is rewritten as

$$\mathbf{i}_{sh0} = \mathbf{G}\mathbf{v}_0 + \sum_{i=1}^{N_y} \check{\mathbf{G}}_i \boldsymbol{\psi}_i \quad (55)$$

where $\check{\mathbf{G}}_i = (\hat{q}_i + 1)\hat{\mathbf{G}}_i$ is a precalculated term. The aforementioned solution steps are now modified to become:

- 1) evaluate (17), $\boldsymbol{\psi}_i = \hat{q}_i \boldsymbol{\psi}'_i + \mathbf{v}'_0$ for all N_y ;
- 2) evaluate $\sum_{i=1}^{N_y} \check{\mathbf{G}}_i \boldsymbol{\psi}_i$ in (55);
- 3) provide the history currents of (30) to the network solution to find \mathbf{v}_0 ;
- 4) prepare for the next timepoint $\boldsymbol{\psi}'_i = \boldsymbol{\psi}_i$ and $\mathbf{v}'_0 = \mathbf{v}_0$.

The number of multiplications and additions per timepoint are given by the same count $N_y * N * (N + 1)$. The gain in the number of operations compared to Method 2 is $(2N + 1)/(N + 1)$.

ACKNOWLEDGMENT

The authors would like to thank J. Bélanger, J.-S. Bejeau, and E. Y. Adjakly of Opal-RT Technologies, Inc., for their contributions and support.

REFERENCES

- [1] J. R. Marti, "Accurate modeling of frequency-dependent transmission lines in electromagnetic transient simulations," *IEEE Trans. Power App. Syst.*, vol. PAS-101, no. 1, pp. 147–157, Jan. 1982.

- [2] X. Wang and R. M. Mathur, "Real-time digital simulator of the electromagnetic transients of transmission lines with frequency dependence," *IEEE Trans. Power Del.*, vol. 4, no. 4, pp. 2249–2255, Oct. 1989.
- [3] C. Dufour, H. Le-Huy, J. C. Soumagne, and A. El Hakimi, "Real-time simulation of power transmission lines using marti model with optimal fitting on dual-DSP card," *IEEE Trans. Power Del.*, vol. 11, no. 1, pp. 412–419, Jan. 1996.
- [4] J. Sousa, M. T. Correia de Barros, and O. Huet, "Frequency-dependent transmission line modelling for a real-time simulator," presented at the Int. Conf. Power System Transients, Seattle, WA, 1997.
- [5] H. M. J. De Silva, A. M. Gole, J. E. Nordstrom, and L. M. Wedepohl, "Robust passivity enforcement scheme for time domain simulation of multi-conductor transmission lines and cables," *IEEE Trans. Power Del.*, vol. 25, no. 2, pp. 930–938, Apr. 2010.
- [6] [Online]. Available: www.mathworks.com. 2012.
- [7] RT-LAB, 2012. [Online]. Available: www.opal-rt.com
- [8] A. Morched, B. Gustavsen, and M. Tartibi, "A universal model for accurate calculation of electromagnetic transients on overhead lines and underground cables," *IEEE Trans. Power Del.*, vol. 14, no. 3, pp. 1032–1038, Jul. 1999.
- [9] B. Gustavsen, G. Irwin, R. Manglørød, D. Brandt, and K. Kent, "Transmission line models for the simulation of interaction phenomena between parallel AC and DC overhead lines," presented at the IPST, Budapest, Hungary, 1999.
- [10] B. Gustavsen and J. Nordstrom, "Pole identification for the universal line model based on trace fitting," *IEEE Trans. Power Del.*, vol. 23, no. 1, pp. 472–479, Jan. 2008.
- [11] B. Gustavsen and J. Mahseredjian, "Simulation of internal overvoltages on transmission lines by an extended method of characteristics approach," *IEEE Trans. Power Del.*, vol. 22, no. 3, pp. 1736–1742, Jul. 2007.
- [12] C. Dufour, J. Mahseredjian, and J. Bélanger, "A combined state-space nodal method for the simulation of power system transients," *IEEE Trans. Power Del.*, vol. 26, no. 2, pp. 928–935, Apr. 2011.
- [13] A. Semlyen and M. Abdel-Rahman, "A state variable approach for the calculation of switching transients on a power transmission line," *IEEE Trans. Circuits Syst.*, vol. CAS-29, no. 9, pp. 624–633, Sep. 1982.
- [14] B. Gustavsen and A. Semlyen, "Rational approximation of frequency domain responses by vector fitting," *IEEE Trans. Power Del.*, vol. 14, no. 3, pp. 1052–1061, Jul. 1999.
- [15] I. Kocar, J. Mahseredjian, and G. Olivier, "Weighting method for transient analysis of underground cables," *IEEE Trans. Power Del.*, vol. 23, no. 3, pp. 1629–1635, Jul. 2008.
- [16] I. Kocar, J. Mahseredjian, and G. Olivier, "Improvement of numerical stability for the computation of transients in lines and cables," *IEEE Trans. Power Del.*, vol. 25, no. 2, pp. 1104–1111, Apr. 2010.
- [17] L. M. Wedepohl, "Electrical characteristics of polyphase transmission systems with special reference to boundary-value calculations at power-line carrier frequencies," in *Proc. Inst. Elect. Eng.*, Nov. 1965, vol. 112, no. 11, pp. 2103–2112.
- [18] F. J. Marcano and J. R. Marti, "Idempotent line model: Case studies," presented at the Int. Conf. Power Syst. Transients, Seattle, WA, Jun. 1997.
- [19] H. W. Bode, *Network Analysis and Feedback Amplifier Design*. London, U.K.: Van Nostrand, 1945.
- [20] J. L. Naredo, J. Mahseredjian, J. A. Gutierrez-Robles, O. Ramos-Leaños, C. Dufour, and J. Belánger, "Improving the numerical performance of transmission line models in EMTP," in *Proc. Int. Conf. Power Syst. Transients*. Delft: the Netherlands, Jun. 2011.
- [21] J. Mahseredjian, S. Denetière, L. Dubé, B. Khodabakhchian, and L. Gérin-Lajoie, "On a new approach for the simulation of transients in power systems," *Elect. Power Syst. Res.*, vol. 77, no. 11, pp. 1514–1520, Sep. 2007.
- [22] L. M. Wedepohl, H. V. Nguyen, and G. D. Irwin, "Frequency-dependent transformation matrices for untransposed transmission lines using Newton-Raphson method," *IEEE Trans. Power Syst.*, vol. 11, no. 3, pp. 1538–1546, Aug. 1996.

Octavio Ramos-Leaños received the M.A.Sc. degree in electrical engineering from Cinvestav-Guadalajara, Guadalajara, Mexico, in 2008 and is currently pursuing the Ph.D. degree in electrical engineering at École Polytechnique de Montréal, Montréal, QC, Canada.

He conducted research-and-development work with Energía e Información (ENERI) Mexico, Zapopan, Jalisco, Mexico, in the area of energy management in 2009. His research interests are related to the study of electromagnetic transients and the simulation of power lines and cables for real-time and offline simulations.

José Luis Naredo (SM'01) received the M.A.Sc. and Ph.D. degrees from the University of British Columbia, Vancouver, BC, Canada, in 1987 and in 1992, respectively.

He conducted research-and-development work at The Electrical Research Institute of Mexico (IIE), Cuernavaca, Morelos, Mexico, in the areas of power system communications, power system transients, and power system protections (from 1978 to 1985 and 1992 to 1994). From 1994 to 1997, he was a Full Professor at the Universidad de Guadalajara, Guadalajara, Mexico. Since 1997, he has been a Full Professor at Cinvestav-Guadalajara, Guadalajara. From 2009 to 2011, he was a Visiting Researcher at École Polytechnique de Montréal, Montréal, QC, Canada.

Jean Mahseredjian (SM'08) received the Ph.D. degree from the École Polytechnique de Montréal, Montréal, QC, Canada, in 1991.

From 1987 to 2004, he was with IREQ (Hydro-Québec), working on research-and-development activities related to the simulation and analysis of electromagnetic transients. In 2004, he joined the Faculty of Electrical Engineering, École Polytechnique de Montréal, Montréal, QC, Canada.

Christian Dufour (M'12) received the Ph.D. degree from Laval University, Laval, QC, Canada, in 2000.

He joined Opal-RT Technologies, Montreal, in 1999, where he has been the Lead Researcher in electric system simulation software for RT-LAB. Before joining Opal-RT, he worked on the development teams of Hydro-Quebec Hypersim real-time simulator as well as the MathWorks' SimPowerSystems blockset. His current research interests are related to the algorithmic solutions for the real-time simulation of power systems and motor drives.

José Alberto Gutiérrez-Robles received the B.Eng. degree in mechanical and electrical engineering, the M.Sc. degrees in power systems from CUCEI-Universidad de Guadalajara, Guadalajara, Mexico, in 1993 and 1998, respectively, and the Ph.D. degree in power systems from Cinvestav, Guadalajara Campus, Guadalajara, Mexico, in 2002.

Currently, he is a Full Professor in the Department of Mathematics, CUCEI, University of Guadalajara. His research interests are in applied mathematics, power system electromagnetic transients, and lightning performance.

Ilhan Kocar (M'10) received the B.Sc. and M.Sc. degrees in electrical and electronics engineering from Orta Dogu Teknik Universitesi, Ankara, Turkey, in 1998 and 2003, respectively, and the Ph.D. degree in electrical engineering from École Polytechnique de Montréal, Montréal, QC, Canada, in 2009.

He was a Project Engineer for Aselsan Electronics Inc. between 1998 and 2004. He was an R&D Engineer for the CYME International T&D (part of Cooper Power Systems) between 2009 and 2011. He joined the faculty of electrical engineering at École Polytechnique de Montréal in 2011. His research interests are power system analysis, modeling, and simulation.